



Application of a microscopic optical potential of chiral effective field theory in (p, d) transfer reactions

Yi-Ping Xu¹ · Si-Lu Chen¹ · Dan-Yang Pang²

Received: 13 September 2023 / Revised: 31 October 2023 / Accepted: 2 November 2023 / Published online: 29 January 2024

© The Author(s), under exclusive licence to China Science Publishing & Media Ltd. (Science Press), Shanghai Institute of Applied Physics, the Chinese Academy of Sciences, Chinese Nuclear Society 2024

Abstract

The microscopic global nucleon–nucleus optical model potential (OMP) proposed by Whitehead, Lim, and Holt, the WLH potential (Whitehead et al., Phys Rev Lett 127:182502, 2021), which was constructed in the framework of many-body perturbation theory with state-of-the-art nuclear interactions from chiral effective field theory (EFT), was tested with (p, d) transfer reactions calculated using adiabatic wave approximation. The target nuclei included both stable and unstable nuclei, and the incident energies reached 200 MeV. The results were compared with experimental data and predictions using the phenomenological global optical potential of Koning and Delaroche, the KD02 potential. Overall, we found that the microscopic WLH potential described the (p, d) reaction angular distributions similarly to the phenomenological KD02 potential; however, the former was slightly better than the latter for radioactive targets. On average, the obtained spectroscopic factors (SFs) using both microscopic and phenomenological potentials were similar when the incident energies were below approximately 120 MeV. However, their difference tended to increase at higher incident energies, which was particularly apparent for the doubly magic target nucleus ^{40}Ca .

Keywords Microscopic optical model potential · (p, d) transfer · Spectroscopic factors

1 Introduction

Single-nucleon transfer reactions such as the (d, p) and (p, d) reactions are valuable tools for studying the single-particle structure of atomic nuclei. In recent years, many studies on transfer reactions with radioactive beams have contributed significantly to our understanding of the evolution of nuclear structures and nuclear astrophysics (see, for instance, the review papers of Refs. [2–4]). Nuclear reaction theories are essential for mediating nuclear structure information and measuring nuclear reaction data. In nearly all the theories for transfer reactions, for instance, the distorted-wave Born

approximation (DWBA) [5, 6], adiabatic wave approximation (ADWA) [7, 8], continuum-discretized coupled-channel method (CDCC) [9–11], and Faddeev equation-based models [12–14], optical model potentials (OMPs) are indispensable model inputs. These OMPs affect the theoretical cross-sections, thus affecting the informal nuclear structure obtained from experimental data [15]. Therefore, reliable OMPs are crucial for the nuclear reaction calculations.

Phenomenological global OMPs such as CH89 [16], KD02 [17], Becchetti–Greenless [18], the more recent WP [19] for nucleons, and the OMPs cited in Refs. [20–25] for deuterons or other nuclei are deduced by fitting the elastic scattering data of a particle within a wide range of incident energies and target masses. Phenomenological global OMPs are widely used for nuclear reaction calculations [26–34]. However, most experimental data concern stable nuclei. Therefore, caution is necessary when applying these phenomenological OMPs to reactions involving exotic isotopes. Microscopic optical potentials, which are based on the more fundamental principles of nuclear many-body interactions, can be more appropriate for describing elastic scattering and transfer reactions simultaneously for

Supported by National Natural Science Foundation of China (Nos. U2067205 and 12205098), National Key Laboratory of Computational Physics (HX02021-35).

✉ Dan-Yang Pang
dypang@buaa.edu.cn

¹ School of Nuclear Science and Engineering, North China Electric Power University, Beijing 102206, China

² School of Physics, Beihang University, Beijing 100191, China

unstable nuclei. Microscopic OMPs for nucleons, such as the Bruyères Jeukenne–Lejeune–Mahaux model potential (the JLMB potential) [35] and the global potential based on the Dirac–Brueckner–Hartree–Fock approach developed by Xu et al. (CTOM [36, 37]), and those for deuteron [38], triton [39], α [40], and heavy-ion [41], among others, are used with increasing frequency in applications to direct nuclear reactions. In addition, microscopic OMPs have been found to be more reliable for extracting nuclear structure information from transfer reaction data [42]. However, many microscopic OMPs are strictly semi-microscopic because some parameters constrained by nucleon scattering data are still present.

It has been found that nucleon elastic scattering and transfer reactions are sensitive to different regions of the OMPs [42]. It is possible that phenomenological OMPs that were constrained only by elastic scattering data (thus, only a certain radial range was well constrained by the experimental data) are not the best for theoretical calculations of transfer reactions. Recently, Whitehead, Lim, and Holt constructed a microscopic global nucleon–nucleus optical potential based on an analysis of 1800 isotopes in the framework of many-body perturbation theory with state-of-the-art nuclear interactions from chiral effective field theory (EFT) [1]. An attractive feature of the WLH potential is that none of its parameters are fitted to the nucleon–nucleus scattering data. One might expect that being derived fully microscopically, the WLH potential might be more suitable for probing nuclear structure information via transfer reactions. Thus, it is necessary to test the WLH potential with (p, d) transfer reactions to compare the results with experimental data and with the same calculations using phenomenological global nucleon–nucleus potentials.

In this study, tests were conducted using 28 sets of (p, d) reaction angular distributions on 15 nuclei, including both stable and unstable nuclei, for incident energies below 200 MeV/nucleon. The global phenomenological nucleon–nucleus potential of Koning and Delaroche (KD02 potential) [17] was used for comparison. The Johnson–Soper adiabatic wave approximation (ADWA) was adapted for the (p, d) and (d, p) reaction calculations. The ADWA, which is essentially a three-body nuclear reaction model, considers the deuteron breakup effect simply but effectively [7]. It is widely used in the analysis of (p, d) and (d, p) reactions (see Refs. [43, 44]). More importantly, it does not involve the deuteron-target OMPs; instead, it considers the deuteron as a $p+n$ system and calculates the distorted waves of the $(p+n)$ -target three-body system with proton- and neutron-target OMPs. Thus, only nucleon-target OMPs are required in the ADWA model, which suits our need to estimate the microscopic WLH potential with (p, d) and (d, p) reactions.

The remainder of this paper is organized as follows: In Sect. 2, we briefly introduce the theoretical model and procedures of data analysis. An analysis of the transfer reactions

is presented in Sect. 3.1. The results for incident energies higher than 150 MeV are presented in Sect. 3.2 and for unstable nuclei are given in Sect. 3.3. A discussion of the spectroscopic factors (SFs) is presented in Sect. 3.4. Finally, we summarize our conclusions in Sect. 4.

2 Methodology

To study the effects of microscopic WLH potential on the cross-section of the transfer reaction, we investigated the (p, d) transfer reactions with 15 target nuclei, which included ^{28}Si , $^{34,46}\text{Ar}$, ^{40}Ca , ^{54}Fe , $^{56,58,60}\text{Ni}$, ^{90}Zr , ^{120}Sn , ^{102}Ru , ^{140}Ce , $^{142,144}\text{Nd}$, and ^{208}Pb . The incident energies varied between 18 and 200 MeV/nucleon. The ranges of the target nuclei and incident energies were mainly limited by the upper bounds of the ranges of incident energies of the WLH and KD02 potentials, the lower bound of the target mass of KD02, and the availability of experimental data. All experimental data were obtained from the nuclear reaction database EXFOR/CSISRS [45] or digitized from original papers, as shown in Tables 1 and 2.

We adopted the three-body model reaction methodology (TBMRM) proposed by Lee et al. to analyze (p, d) reactions [43, 44, 72]. This methodology uses the Johnson–Soper ADWA model for the (p, d) and (d, p) reactions [7], where the amplitude of the $A(p, d)B$ reaction is given by [73]

$$T_{pd} = SF_{nlj}^{1/2} \langle \chi_{dB}^{(-)} \phi_{np} | V_{np} | \chi_{pA}^{(+)} \phi_{nlj} \rangle, \quad (1)$$

where SF_{nlj} is the spectroscopic with n , l , and j being the node number, angular momentum, and total angular momentum, respectively, of the single-neutron wave function ϕ_{nlj} in the nucleus A ($A = B + n$); χ_{pA} and χ_{dB} are the entrance- and exit-channel distorted waves, respectively; and V_{np} is the neutron–proton interaction that supports the bound state of the n - p pair ϕ_{np} (the deuteron wave function).

In this work, V_{np} is the Gaussian potential with a depth of 72.15 MeV and a radius of 1.484 fm, which is taken from Ref. [74]. With this potential, only the s -wave was considered in ϕ_{np} . Using the ADWA model, exit-channel distorted waves are generated with the following effective “deuteron” (as a subsystem composed of neutrons and protons) potential [7, 8]:

$$U_{dB}(R) = \frac{\langle \phi_{np} | V_{np} \left[U_{nB}(\mathbf{R} + \frac{\mathbf{r}}{2}) + U_{pB}(\mathbf{R} - \frac{\mathbf{r}}{2}) \right] | \phi_{np} \rangle}{\langle \phi_{np}(\mathbf{r}) | V_{np}(\mathbf{r}) | \phi_{np}(\mathbf{r}) \rangle}, \quad (2)$$

where U_{nB} and U_{pB} are the neutron and proton OMPs on the target nucleus B evaluated at half of the deuteron incident energies (the “ $E_d/2$ rule”). In the zero-range version of ADWA, the effective deuteron potential becomes

Table 1 Spectroscopic factors (SFs) obtained with the WLH and KD02 potentials for stable isotopes at different energies

Target	E_p (MeV)	References	SF _{WLH}	SF _{KD02}
²⁸ Si	33.6	[46]	3.353	3.495
	51.93	[47]	3.491	3.727
	185	[48]	1.928	1.419
⁴⁰ Ca	27.5	[49]	2.570	2.666
	65	[50]	2.568	2.809
	156	[51]	4.364	2.530
	185	[52]	4.482	2.183
	200	[53]	4.114	1.794
⁵⁴ Fe	51.93	[54]	2.724	3.179
	122.4	[55]	3.187	3.241
⁵⁸ Ni	24.6	[56]	1.222	1.270
	51.93	[57]	1.113	0.992
	65	[58]	1.251	0.870
⁶⁰ Ni	94	[59]	1.091	0.853
⁹⁰ Zr	58	[60]	4.855	5.250
	90	[61]	5.296	6.948
	121.2	[62]	5.772	6.234
¹⁰² Ru	26.3	[63]	1.803	1.953
¹²⁰ Sn	18	[64]	2.033	1.903
	26.3	[65]	0.587	0.619
¹⁴⁰ Ce	55.05	[66]	2.289	2.029
¹⁴² Nd	52	[67]	9.358	8.573
¹⁴⁴ Nd	22	[68]	2.147	2.154
	22	[68]	0.703	1.174
²⁰⁸ Pb	22	[68]	0.703	1.174
	65	[69]	7.018	4.662

The reference to the experimental dataset used in the extraction is also listed

Table 2 SFs obtained with the WLH and KD02 potentials for unstable isotopes at different energies

Target	E_p (MeV)	References	SF _{WLH}	SF _{KD02}
³⁴ Ar	33	[70]	0.876	0.787
⁴⁶ Ar	33	[70]	4.615	5.541
⁵⁶ Ni	37	[71]	5.380	7.502

The reference to the experimental dataset used in the extraction is also listed

$$U_{dB}(R) = U_{nB}(R) + U_{pB}(R). \quad (3)$$

Clearly, with the three-body ADWA model, only the neutron and proton OMPs are required. This allows the calculation of the (p, d) and (d, p) reactions using only one set of systematic OMPs. Zero-range ADWA was found to be satisfactory for describing the deuteron pickup and stripping reactions [43, 44]. Therefore, although the finite-range version of the ADWA model and more sophisticated yet complicated

continuum-discretized coupled-channel models are available for the analysis of (d, p) reactions [8, 73], we adopted the zero-range ADWA model in this study. To examine the microscopic WLH potential and compare its results with the phenomenological KD02 potential, zero-range ADWA should be sufficient.

The single-particle wave functions were calculated using the separation energy prescription with the Woods–Saxon form of the single-particle potentials. The depths of these potentials were adjusted to reproduce the neutron separation energies in the ground state of the target nuclei. The radius and diffuseness parameters of these potentials, r_0 and a_0 , are also important for the nuclear transfer reactions. Their empirical values were $r_0 = 1.25$ fm and $a_0 = 0.65$ fm. However, these empirical values do not represent the specific structure of a single nucleus. A better solution is to confine the r_0 and a_0 values with a reliable nuclear structure theory. The TBMRM constrains the r_0 and a_0 values using modern Hartree–Fock (HF) calculations [43, 72, 72, 75–83]. Using this procedure, the diffuseness parameter was fixed at $a_0 = 0.7$ fm. The radius parameter r_0 was determined by requiring the root-mean-square (rms) radius of the single-neutron wave function, $\sqrt{\langle r^2 \rangle}$, to be related with the rms radius of the corresponding single-particle orbital from HF calculations, $\sqrt{\langle r^2 \rangle_{\text{HF}}}$, by $\langle r^2 \rangle = [A/(A - 1)] \langle r^2 \rangle_{\text{HF}}$. The factor $[A/(A - 1)]$ was used to correct the fixed potential center assumption used in the HF calculations, where A is the mass number of the composite nucleus. All the HF calculations performed in this work were based on the SkX interaction [84]. We adopted the same procedure as that used in our previous studies [42, 81]. All transfer differential cross-sections were calculated using the TWOFNR code [85].

3 Results and discussion

3.1 Transfer reactions on stable nuclei at low energies

The reliability of the WLH potential for the (p, d) transfer reactions was first checked with stable nuclei at incident energies $E_p \leq 150$ MeV, which fall within the range of incident energies of the WLH potential. The target nuclei included ²⁸Si, ⁴⁰Ca, ⁵⁴Fe, ^{58,60}Ni, ⁹⁰Zr, ¹²⁰Sn, ¹⁰²Ru, ¹⁴⁰Ce, ^{142,144}Nd, and ²⁰⁸Pb. The results are shown in Figs. 1–3 together with the experimental data. For comparison, the results calculated using the global phenomenological KD02 potential are also presented. All the calculated results were normalized to the experimental data at the first peaks of the angular distributions or at the angles where the maximum measured differential cross-sections occurred. Neutron SFs were obtained using this procedure. All experimental data correspond to neutron transfer from the ground states of the

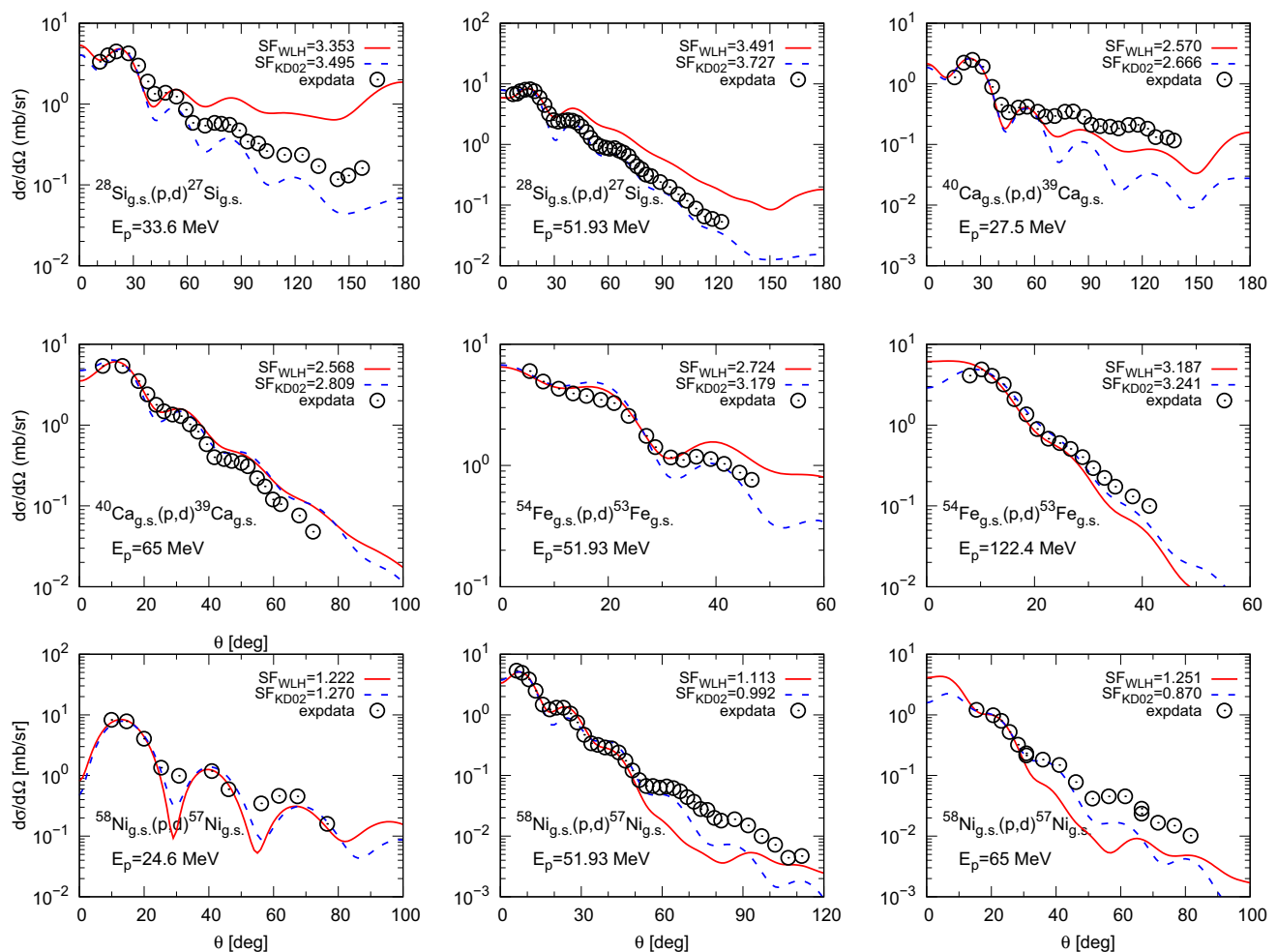


Fig. 1 (Color online) Comparisons between the two optical model calculations and experimental data of (p, d) reactions on ^{28}Si , ^{40}Ca , ^{54}Fe , and ^{58}Ni at the incident energies, up to 150 MeV, indicated in

the figures. The solid and dashed curves are calculated with the WLH and KD02 potentials, respectively. The values of the differential cross-sections are multiplied by the corresponding SF as labeled

target nuclei to the ground states of the residual nuclei; thus, the results obtained in this work are single-neutron SFs in the ground states of the target nuclei.

As shown in Figs. 1, 2, and 3, generally, the experimental data can be satisfactorily reproduced by the WLH potential at forward angles as well as by the KD02 potential. The WLH potential was even better than the KD02 potential in some cases, such as $^{120}\text{Sn}_{\text{g.s.}}(p, d)^{119}\text{Sn}_{\text{g.s.}}$ at 18 MeV. In some individual cases, the experimental angular distributions were not reproduced satisfactorily using either OMPs, for example, $^{120}\text{Sn}_{\text{g.s.}}(p, d)^{119}\text{Sn}_{\text{g.s.}}$ at 26.3 MeV. Problems other than the OMP may exist in these cases.

3.2 Extrapolation to higher energies

The WLH potential is expected to work for incident energies below 150 MeV. Above this energy range, the theoretical uncertainties may become uncontrolled. However, it is

interesting to observe how this operates when extrapolated to higher energies. When the incident energies are higher than approximately 150 MeV, the randomly generated WLH potential may generate unphysical positive potential. In these cases, we set the number of random pulls to 1500, which allowed us to obtain the least 1000 negative-valued potentials from which we could obtain reasonable averaged potentials. In Fig. 4, we show results for (p, d) reactions on ^{28}Si and ^{40}Ca targets at incident energies between 150 and 200 MeV. Again, it can be observed that the WLH potential reasonably reproduced these higher-energy data and yielded results very close to those of the KD02 potential at forward angles.

3.3 Transfer reactions on unstable nuclei

There is a pressing need for high-quality optical potentials for nuclei that are far from stable, which represent a frontier

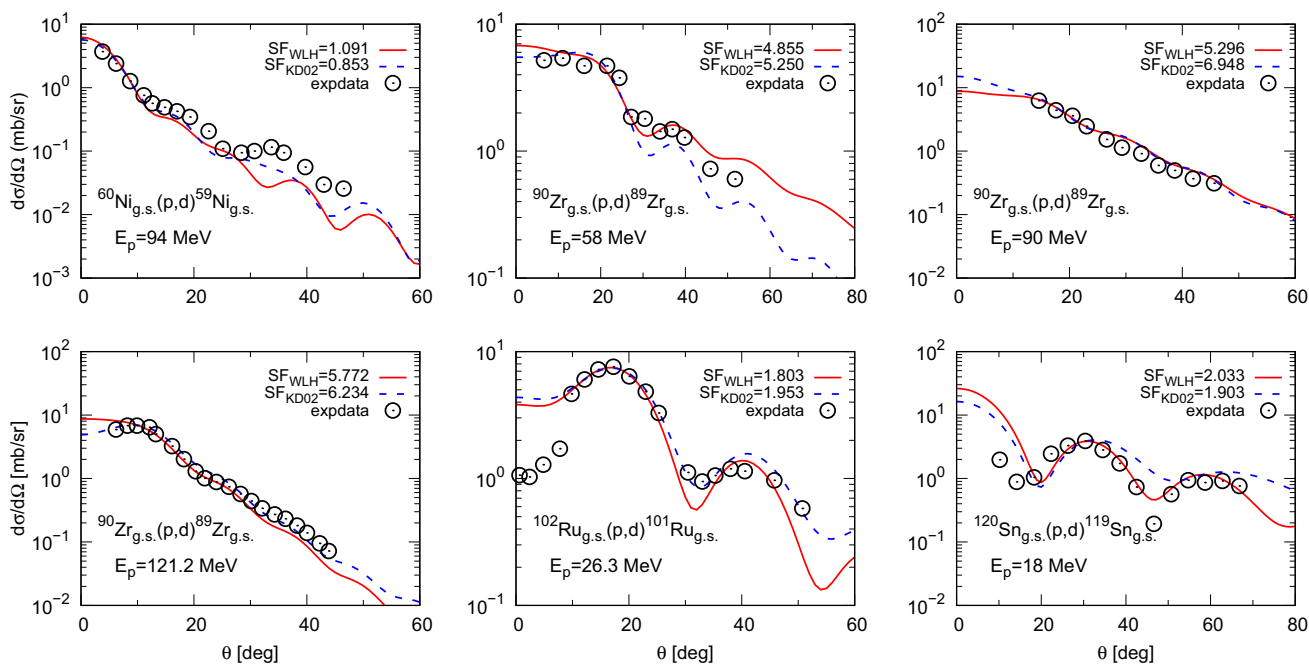


Fig. 2 (Color online) Same comparison as that in Fig. 1 but on ^{60}Ni , ^{90}Zr , ^{102}Ru , and ^{120}Sn

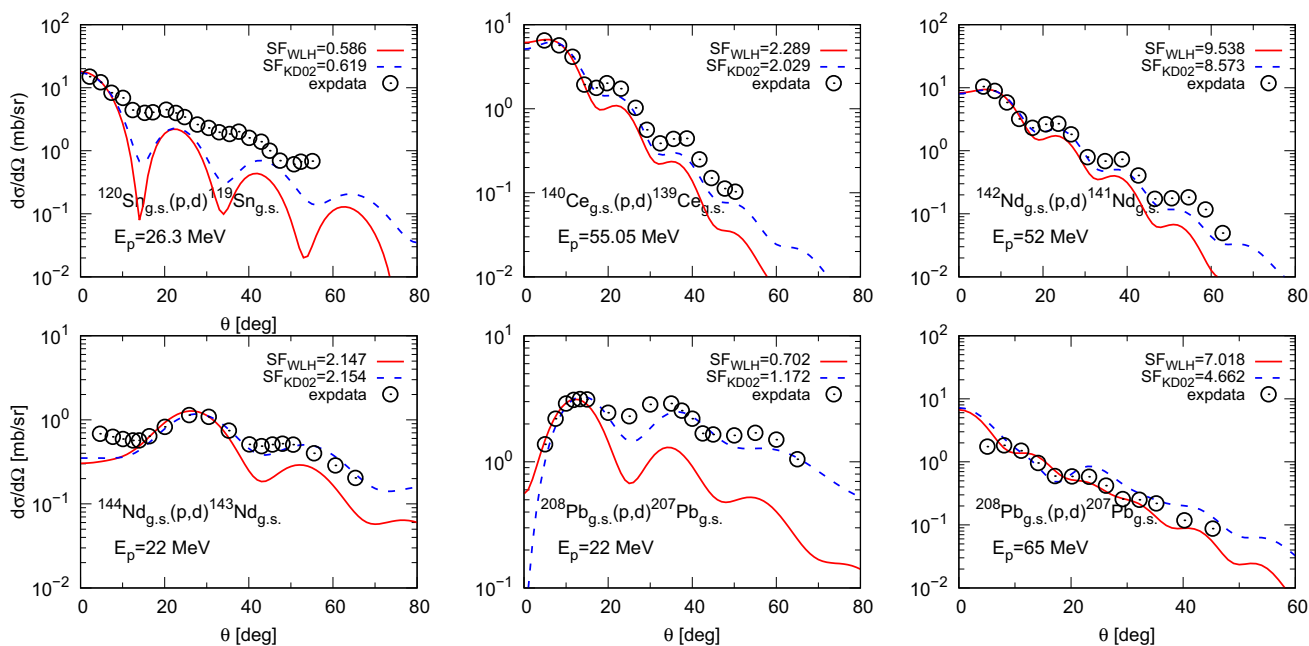
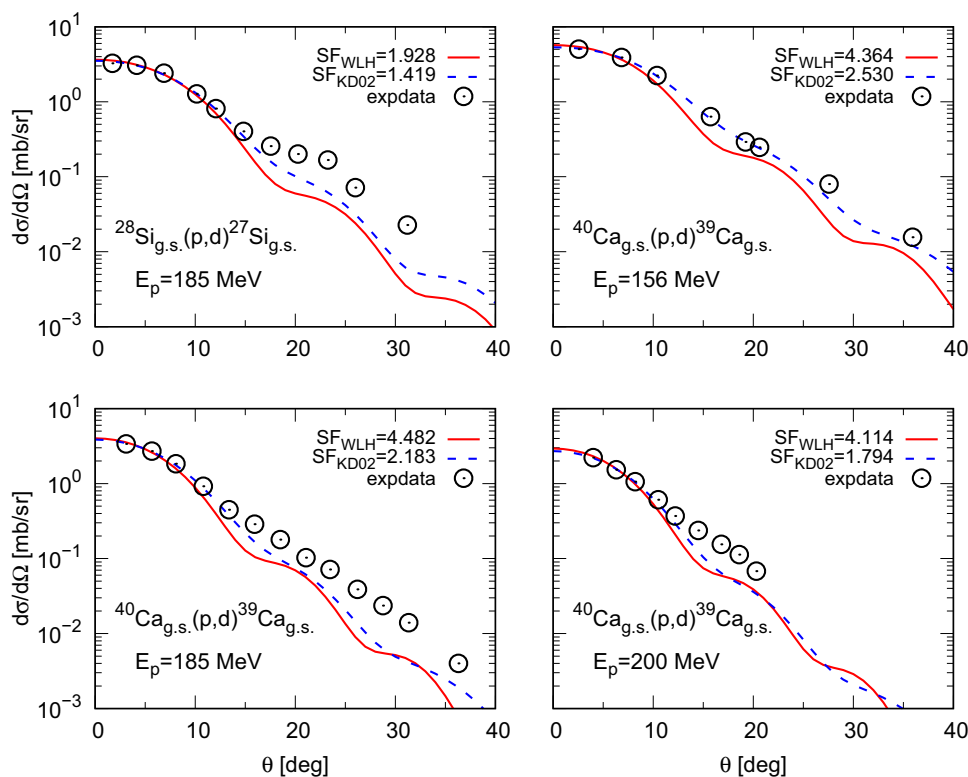


Fig. 3 (Color online) Same comparison as that in Fig. 1 but on ^{120}Sn , ^{140}Ce , $^{142,144}\text{Nd}$, and ^{208}Pb

in nuclear physics [86–88]. Phenomenological potentials are most suitable for reactions where the masses of the target nuclei are within the mass range of the experimental database from which the potential parameters are constrained. Because most elastic scattering data used to obtain phenomenological OMPs were measured on stable targets, the

resulting OMP parameters may be biased by the limited range of target masses in the database. Therefore, caution is always advised when extrapolating these potentials to unstable nuclei, particularly when they are far from the β stability line. Meanwhile, microscopic OMPs, which are derived from effective nucleon–nucleon interactions with reliable

Fig. 4 (Color online) Comparisons between two optical model calculations and experimental data of (p, d) reactions on ^{28}Si and ^{40}Ca at the incident energies >150 MeV indicated in the figures. The solid and dashed curves are calculated with the WLH and KD02 potentials, respectively. The values of the differential cross-sections are multiplied by the corresponding SF as labeled



nuclear structure models, are expected to be more sophisticated when applied to reactions with unstable nuclei. It is interesting to examine how the microscopic WLH potential works on unstable nuclei, and how it compares with the phenomenological KD02 potential. The results are presented in Fig. 5 for (p, d) reactions on unstable targets $^{34,46}\text{Ar}$ and ^{56}Ni . As can be observed, again, the WLH potential reproduced the experimental data reasonably well. In the ^{56}Ni case, the WLH potential was even slightly better than the KD02 potential. Unfortunately, the experimental data for (p, d) reactions on unstable nuclei are limited. More measurements of the (p, d) reaction data on targets further away from the β -stability line are required to examine the applicability of the WLH potential.

3.4 Spectroscopic factors

The OMPs affect not only the angular distributions but also the magnitudes of the (p, d) reactions. Both aspects of experimental data are important in nuclear reaction studies. Comparisons between the theoretical and experimental angular distributions determine whether the assumed reaction mechanism in the theoretical model and their parameters are appropriate, whereas the magnitudes of (p, d) reactions determine the SFs that provide important information about the nuclear single-particle structure. As stated above, the SFs are extracted experimentally by matching the theoretical and experimental angular distributions at the maximum cross-sections, where the uncertainties of the experimental

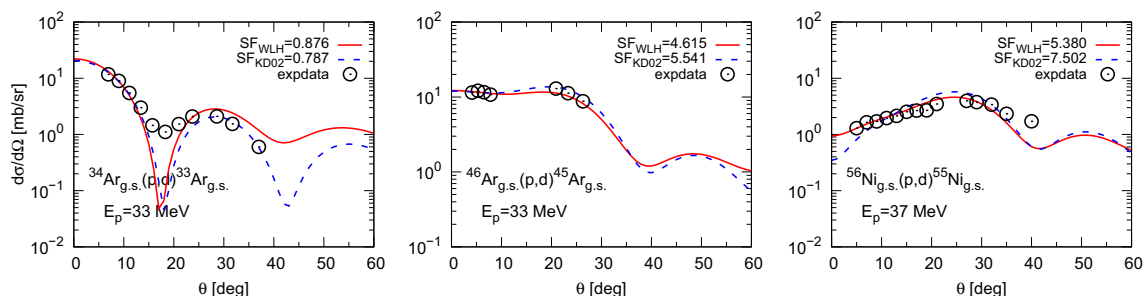


Fig. 5 (Color online) Comparisons between two optical model calculations and experimental data of (p, d) reactions on unstable nuclei, including ^{34}Ar , ^{46}Ar , and ^{56}Ni , at the incident energies indicated in

the figures. The solid and dashed curves are calculated with the WLH and KD02 potentials, respectively. The values of the differential cross-sections are multiplied by the corresponding SF as labeled

data and the extracted SFs are at their minimum [70] (see Figs. 1, 2, 3, 4, and 5). The SFs from all reactions analyzed in this study are presented in Tables 1 and 2.

Comparisons between the SFs obtained using the microscopic WLH potential and the phenomenological KD02 potential are shown in Fig. 6 for their ratios, SF_{WLH}/SF_{KD02} , at different incident energies. The target nuclei included are the doubly magic isotopes ^{40}Ca and ^{208}Pb , stable nuclei ^{28}Si , $^{58,60}\text{Ni}$, ^{90}Zr , ^{120}Sn , ^{102}Ru , ^{140}Ce , and $^{142,144}\text{Nd}$, and unstable

nuclei $^{34,46}\text{Ar}$ and ^{56}Ni . Interestingly, when the incident energy was less than approximately 120 MeV, the two systematic potentials gave, on average, very similar SFs for all types of nuclei. However, when the range of incident energies increased to approximately 200 MeV, the ratios showed an increasing trend. This is especially apparent for the doubly magic nucleus ^{40}Ca (there is a lack of experimental data for ^{208}Pb above 100 MeV). When the results in the tables are examined, it can be observed that the changes in SFs of ^{40}Ca with the KD02 potential are much smaller over the ranges of incident energies than those with the WLH potential.

It is well known that OMPs with doubly magic nuclei do not follow the systematics of OMPs established for other nuclei because of the relatively larger excitation energies of their first few excited states [16, 22, 94]. The increased disagreement between the SFs and the WLH and KD02 potentials at higher energies may indicate deficiencies in these potentials. Therefore, we compared the descriptions of proton elastic scattering from ^{40}Ca at higher energies. The results are presented in Fig. 7 for the ^{40}Ca target. It can be observed that, at lower energies, the two potentials describe the experimental data similarly. However, at higher energies, the phenomenological KD02 potential appears to be better than the microscopic WLH potential. However, neither potential reproduced the higher-energy data nor the low-energy data. Because all other parameters are the same in the transfer reaction calculations, this could be the reason for the differences among the SFs obtained at both potentials.

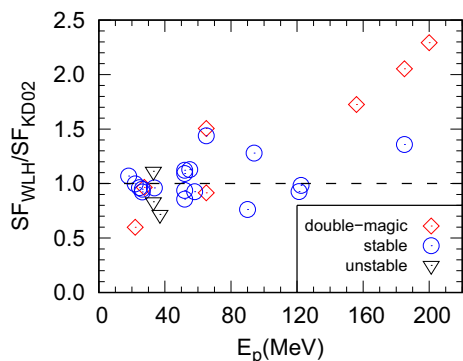


Fig. 6 (Color online) Ratios of experimental ground-state neutron SF values between the WLH and KD02 calculations as a function of mass number. The dashed line indicates a perfect agreement between data and theory. Open diamonds, open circles, and open triangles denote SF ratios extracted from (*p, d*) reactions on doubly magic nuclei, stable nuclei (not doubly magic), and unstable nuclei, respectively

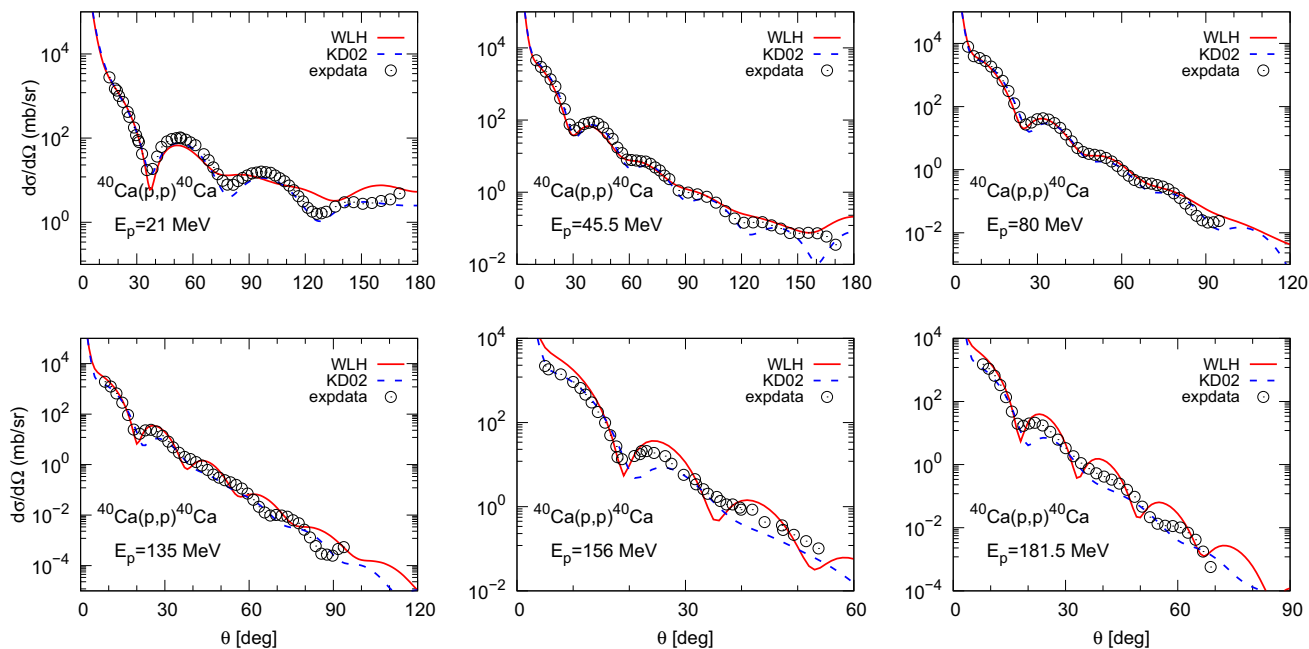


Fig. 7 (Color online) Comparison of the elastic scattering reaction cross-section of the WLH calculation (solid lines), KD calculation (dashed lines), and experimental data (points) from Refs. [89–93] for $p+^{40}\text{Ca}$

Note that these incident energies are outside the range of WLH, which is for $E_p < 150$ MeV. This suggests that caution is needed when extrapolating the WLH potentials at higher incident energies. Meanwhile, improvement of the systematic potential to lighter targets and/or higher-energy regions would be interesting and useful, especially for doubly magic nuclei.

4 Summary

We verified the performance of the new microscopic optical WLH potential based on EFT theory in (p , d) reactions. In the present study, we performed zero-range adiabatic calculations for 15 nuclei, covering a wide range of 18–200 MeV/nucleon. The phenomenological KD02 potential parameters were used for comparison. This pure microscopic optical potential effectively reproduced the angular distributions of both stable and unstable nuclei as well as the phenomenological KD02 potential. Our results suggest that the microscopic WLH potential can be used as an advanced approach for the prediction of transfer reactions on unstable nuclei and for extracting nuclear structure information of exotic nuclei.

Furthermore, we studied the amplitudes of the transfer cross-sections with the WLH potential. The SFs extracted using the WLH potential were close to those obtained using the KD02 potential for all types of nuclei below approximately 120 MeV. However, when the range of incident energies was increased to approximately 200 MeV, the ratios showed a significant increasing trend with an increase in incident energy, especially for the doubly magic nucleus ^{40}Ca case. Comparisons between the WLH and KD02 potentials in their descriptions of proton elastic scattering from ^{40}Ca were performed up to 200 MeV. The results showed that some imperfections existed at higher energies for both potentials. An improvement in the WLH potential at higher incident energies for doubly magic nuclei is expected. Nevertheless, in general, the successful application of the WLH potential in (p , d) transfer reactions seems encouraging.

Author Contributions All authors contributed to the study conception and design. Material preparation, data collection, and analysis were performed by Yi-Ping Xu, Si-Lu Chen, and Dan-Yang Pang. The first draft of the manuscript was written by Yi-Ping Xu, and all authors commented on the previous versions of the manuscript. All authors read and approved the final manuscript.

Data availability The data that support the findings of this study are openly available in Science Data Bank at <https://cstr.cn/31253.11.sciencedb.14619> and <https://www.doi.org/10.57760/sciencedb.14619>.

Declarations

Conflict of interest The authors declare that they have no competing interests.

References

1. T.R. Whitehead, Y. Lim, J.W. Holt, Global microscopic description of nucleon-nucleus scattering with quantified uncertainties. *Phys. Rev. Lett.* **127**, 182502 (2021). <https://doi.org/10.1103/PhysRevLett.127.182502>
2. D.W. Bardayan, Transfer reactions in nuclear astrophysics. *J. Phys. G Nucl. Part. Phys.* **43**, 043001 (2016). <https://doi.org/10.1088/0954-3899/43/4/043001>
3. K. Wimmer, Nucleon transfer reactions with radioactive beams. *J. Phys. G Nucl. Part. Phys.* **45**, 033002 (2018). <https://doi.org/10.1088/1361-6471/aaa2bf>
4. N.K. Timofeyuk, R.C. Johnson, Theory of deuteron stripping and pick-up reactions for nuclear structure studies. *Prog. Part. Nucl. Phys.* **127**, 103738 (2020). <https://doi.org/10.1016/j.ppnp.2019.103738>
5. G.R. Satchler (ed.), *Direct Nuclear Reactions* (Oxford University Press Inc., New York, 1983)
6. Q.B. Shen (ed.), *Low- and Intermediate-Energy Direct Nuclear Reaction Theories* (Science Press, Beijing, 2005)
7. R.C. Johnson, P.J.R. Soper, Contribution of deuteron breakup channels to deuteron stripping and elastic scattering. *Phys. Rev. C* **1**, 976–990 (1970). <https://doi.org/10.1103/PhysRevC.1.976>
8. R.C. Johnson, P.C. Tandy, An approximate three-body theory of deuteron stripping. *Nucl. Phys. A* **235**, 56–74 (1974). <https://www.sciencedirect.com/science/article/pii/037594747490178X>. [https://doi.org/10.1016/0375-9474\(74\)90178-X](https://doi.org/10.1016/0375-9474(74)90178-X)
9. M. Kamimura et al., Chapter I. Projectile breakup processes in nuclear reactions. *Prog. Theor. Phys. Suppl.* **89**, 1–10 (1986). <https://doi.org/10.1143/PTPS.89.1>
10. N. Austern, Y. Iseri, M. Kamimura et al., Continuum-discretized coupled-channels calculations for three-body models of deuteron-nucleus reactions. *Phys. Rep.* **154**, 125–204 (1987). <https://www.sciencedirect.com/science/article/abs/pii/0370157387900949>. [https://doi.org/10.1016/0370-1573\(87\)90094-9](https://doi.org/10.1016/0370-1573(87)90094-9)
11. M. Yahiro, K. Ogata, T. Matsumoto et al., The continuum discretized coupled-channels method and its applications. *Prog. Theor. Exp. Phys.* **2012**, 01A206 (2012). <https://academic.oup.com/ptep/article/2012/1/01A206/1560069>. <https://doi.org/10.1093/ptep/pts008>
12. E.O. Alt, P. Grassberger, W. Sandhas, Reduction of the three-particle collision problem to multi-channel two-particle Lippmann-Schwinger equations. *Nucl. Phys. B* **2**, 167–18 (1967). <https://www.sciencedirect.com/science/article/abs/pii/0550321367900168>. [https://doi.org/10.1016/0550-3213\(67\)90016-8](https://doi.org/10.1016/0550-3213(67)90016-8)
13. E.O. Alt, W. Sandhas, H. Ziegelmann, Coulomb effects in three-body reactions with two charged particles. *Phys. Rev. C* **17**, 1981–2005 (1978). <https://doi.org/10.1103/PhysRevC.17.1981>
14. E.O. Alt, L.D. Blokhintsev, A.M. Mukhamedzhanov et al., Deuteron elastic scattering and stripping processes off ^{12}C as a three-body problem. *Phys. Rev. C* **75**, 054003 (2007). <https://doi.org/10.1103/PhysRevC.75.054003>
15. W.J. Kong, D.Y. Pang, Theoretical uncertainties of ($d,3\text{He}$) and ($3\text{He}, d$) reactions owing to the uncertainties of optical model potentials. *Nucl. Sci. Tech.* **34**, 95 (2023). <https://doi.org/10.1007/s41365-023-01242-y>
16. R.L. Varner, W.J. Thompson, T.L. McAbee et al., A global nucleon optical model potential. *Phys. Rep.* **201**, 57–119 (1991). [https://doi.org/10.1016/0370-1573\(91\)90039-O](https://doi.org/10.1016/0370-1573(91)90039-O)
17. A.J. Koning, J.P. Delaroche, Local and global nucleon optical models from 1 keV to 200 MeV. *Nucl. Phys. A* **713**, 231–310 (2003). [https://doi.org/10.1016/S0375-9474\(02\)01321-0](https://doi.org/10.1016/S0375-9474(02)01321-0)
18. F.D. Becchetti, G.W. Greenlees, Nucleon-nucleus optical-model parameters, $A > 40$, $E < 50$ MeV. *Phys. Rev.* **182**, 1190–1209 (1969). <https://doi.org/10.1103/PhysRev.182.1190>

19. S.P. Weppner, R.B. Penney, G.W. Diffendale et al., Isospin dependent global nucleon-nucleus optical model at intermediate energies. *Phys. Rev. C* **80**, 034608 (2009). <https://doi.org/10.1103/PhysRevC.80.034608>
20. H.X. An, C.H. Cai, Global deuteron optical model potential for the energy range up to 183 MeV. *Phys. Rev. C* **73**, 054605 (2006). <https://doi.org/10.1103/PhysRevC.73.054605>
21. X.H. Li, C.T. Liang, C.H. Cai, Global triton optical model potential. *Nucl. Phys. A* **789**, 103–113 (2007). <https://www.sciencedirect.com/science/article/pii/S0375947407002291>. <https://doi.org/10.1016/j.nuclphysa.2007.03.004>
22. D.Y. Pang, P. Roussel-Chomaz, H. Savajols et al., Global optical model potential for $A = 3$ projectiles. *Phys. Rev. C* **79**, 024615 (2009). <https://doi.org/10.1103/PhysRevC.79.024615>
23. Y.L. Xu, H.R. Guo, Y.L. Han et al., Helium-3 global optical model potential with energies below 250 MeV. *Sci. China-Phys. Mech. Astron.* **54**, 2005 (2011). <https://doi.org/10.1007/s11433-011-4488-5>
24. Y. Zhang, D.Y. Pang, J.L. Lou, Optical model potential for deuteron elastic scattering with 1p-shell nuclei. *Phys. Rev. C* **94**, 014619 (2016). <https://doi.org/10.1103/PhysRevC.94.014619>
25. Y.L. Xu, Y.L. Han, X.W. Su et al., Global optical model potential describing the ^{12}C -nucleus elastic scattering. *Chin. Phys. C* **44**, 124103. <https://doi.org/10.1088/1674-1137/abb4d0>
26. X.D. Liu, M.A. Famiano, W.G. Lynch et al., Systematic extraction of spectroscopic factors from $^{12}\text{C}(d, p)^{13}\text{C}$ and $^{13}\text{C}(p, d)^{12}\text{C}$ reactions. *Phys. Rev. C* **69**, 064313 (2004). <https://doi.org/10.1103/PhysRevC.69.064313>
27. J. Lee, D.Y. Pang, Y.L. Han et al., Proton spectroscopic factors deduced from helium-3 global phenomenological and microscopic optical model potentials. *Chin. Phys. Lett.* **31**, 092103 (2014). <https://doi.org/10.1088/0256-307X/31/9/092103>
28. S. Nakayama, Y. Watanabe, Systematic investigation of spectroscopic factors from (d, p) reactions for deuteron nuclear data evaluation. *J. Nucl. Sci. Technol.* **53**, 89–101 (2016). <https://doi.org/10.1080/00223131.2015.1023380>
29. F.S. Olise, O.I. Oladunjoye, A. Ajala et al., Response of multi-step compound pre-equilibrium reaction cross sections for the (p, n) reactions to forms of optical model parameters. *Nucl. Sci. Tech.* **28**, 147 (2017). <https://doi.org/10.1007/s41365-017-0298-4>
30. Y.P. Xu, D.Y. Pang, X.Y. Yun et al., Possible determination of high-lying single-particle components with (p, d) reactions. *Phys. Rev. C* **98**, 04462 (2018). <https://doi.org/10.1103/PhysRevC.98.044622>
31. G.B. King, A.E. Lovell, F.M. Nunes, Uncertainty quantification due to optical potentials in models for (d, p) reactions. *Phys. Rev. C* **98**, 044623 (2018). <https://doi.org/10.1103/PhysRevC.98.044623>
32. H.R. Guo, Y.L. Han, C.H. Cai, Theoretical calculation and evaluation of $n + ^{240,242,244}\text{Pu}$ reactions. *Nucl. Sci. Tech.* **30**, 13 (2019). <https://doi.org/10.1007/s41365-018-0533-7>
33. W. Liu, J.L. Lou, Y.L. Ye et al., Experimental study of intruder components in light neutron-rich nuclei via single-nucleon transfer reaction. *Nucl. Sci. Tech.* **31**, 20 (2020). <https://doi.org/10.1007/s41365-020-0731-y>
34. Y. Gao, Z.Z. Ren, L. Jin, Systematic study of global optical model potentials in (d, p) transfer reactions. *Chin. Phys. C* **47**, 044105 (2023). <https://doi.org/10.1088/1674-1137/acb2bc>
35. J.P. Jeukenne, A. Lejeune, C. Mahaux, Optical-model potential in finite nuclei from Reid's hard core interaction. *Phys. Rev. C* **16**, 80–96 (1970). <https://doi.org/10.1103/PhysRevC.16.80>
36. R.R. Xu, Z.Y. Ma, E.N.E. van Dalen et al., Relativistic nucleon optical potentials with isospin dependence in a Dirac-Brueckner-Hartree-Fock approach. *Phys. Rev. C* **85**, 034613 (2012). <https://doi.org/10.1103/PhysRevC.85.034613>
37. R.R. Xu, Z.Y. Ma, Y. Zhang et al., Global analysis of isospin dependent microscopic nucleon-nucleus optical potentials in a Dirac-Brueckner-Hartree-Fock approach. *Phys. Rev. C* **94**, 034606 (2016). <https://doi.org/10.1103/PhysRevC.94.034606>
38. H.R. Guo, Y.L. Han, Q.B. Shen, A microscopic optical potential for deuteron. *Chin. Phys. Lett.* **27**, 012401 (2010). <https://doi.org/10.1088/0256-307X/27/1/012401>
39. H.R. Guo, Y.L. Xu, H.Y. Liang et al., Microscopic optical model potential for triton. *Nucl. Phys. A* **922**, 84 (2014). <https://www.sciencedirect.com/science/article/abs/pii/S0375947413007896>. <https://doi.org/10.1016/j.nuclphysa.2013.11.007>
40. W. Zou, Y. Tian, Z.Y. Ma, Microscopic optical potential for α -nucleus elastic scattering in a Dirac-Brueckner-Hartree-Fock approach. *Phys. Rev. C* **78**, 064613 (2008). <https://doi.org/10.1103/PhysRevC.78.064613>
41. I. Ochala, J.O. Fiase, B3Y-FETAL effective interaction in the folding analysis of elastic scattering of $^{16}\text{O} + ^{16}\text{O}$. *Nucl. Sci. Tech.* **32**, 81 (2021). <https://doi.org/10.1007/s41365-021-00920-z>
42. X.Y. Yun, D.Y. Pang, Y.P. Xu et al., What kind of optical model potentials should be used for deuteron stripping reactions? *Sci. China-Phys. Mech. Astron.* **63**, 222011 (2020). <https://doi.org/10.1007/s11433-019-9389-6>
43. J. Lee, J.A. Tostevin, B.A. Brown, Reduced neutron spectroscopic factors when using potential geometries constrained by Hartree-Fock calculations. *Phys. Rev. C* **73**, 044608 (2006). <https://doi.org/10.1103/PhysRevC.73.044608>
44. J. Lee, M.B. Tsang, W.G. Lynch, Neutron spectroscopic factors from transfer reactions. *Phys. Rev. C* **75**, 064320 (2007). <https://doi.org/10.1103/PhysRevC.75.064320>
45. EXFOR/CSISRS, Experimental nuclear reaction data. <https://www-nds.iaea.org/exfor/>
46. R.L. Kozub, (p, d) reaction on $N = Z$ nuclei in the $2s - 1d$ shell. *Phys. Rev.* **172**, 1078–1094 (1968). <https://doi.org/10.1103/PhysRev.172.1078>
47. H. Ohnuma, J. Kasagi, F. Kakimoto et al., Forbidden (p, d) transition and their CCBA analysis. *J. Phys. Soc. Jpn.* **48**, 1812–1820 (1980). <https://doi.org/10.1143/JPSJ.48.1812>
48. A. Ingemarsson, G. Tibell, Optical model analysis of proton and deuteron scattering and DWBA calculations on (p, d)-reactions at 185 MeV. *Phys. Scr.* **10**, 159 (1974). <https://doi.org/10.1088/0031-8949/10/4/002>
49. J. Dobeš, An absorption model for direct transfer reactions. *Nucl. Phys. A* **157**, 661–672 (1970). [https://doi.org/10.1016/0375-9474\(70\)90240-X](https://doi.org/10.1016/0375-9474(70)90240-X)
50. P.G. Roos, S.M. Smith, V.K.C. Cheng et al., The (p, d) reaction at 65 MeV. *Nucl. Phys. A* **255**, 187–203 (1975). [https://doi.org/10.1016/0375-9474\(75\)90157-8](https://doi.org/10.1016/0375-9474(75)90157-8)
51. D.A. du texte Bachelier, M. Bernas, I. Brissaud et al., Réaction (p, d) à 156 MeV et structure des noyaux légers. *Nucl. Phys.* **126**, 60–96 (1969). <https://www.sciencedirect.com/science/article/abs/pii/S037594746990400X>. [https://doi.org/10.1016/0375-9474\(69\)90400-X](https://doi.org/10.1016/0375-9474(69)90400-X)
52. J. Källne, B. Fagerström, Studies of (p, d) reactions in ^{24}Mg , ^{32}S and ^{40}Ca at 185 MeV. *Phys. Scr.* **11**, 79–93 (1975). <https://doi.org/10.1088/0031-8949/11/2/002>
53. R. Abegg, D.A. Hutcheon, C.A. Miller et al., Cross section and analyzing power measurements for the (p, d) reaction on ^{16}O and ^{40}Ca at 200 MeV. *Nucl. Phys. C* **39**, 65–69 (1989). <https://doi.org/10.1103/PhysRevC.39.65>
54. H. Ohnuma, T. Suehiro, Y. Ishizaki et al., The $^{54}\text{Fe}(p, d)^{53}\text{Fe}$ reaction at 52 MeV. *J. Phys. Soc. Jpn.* **32**, 1466–1471 (1972). <https://doi.org/10.1143/JPSJ.32.1466>
55. S.A. Dickey, J.J. Kraushaar, J.R. Shepard et al., The $^{54}\text{Fe}(p, d)^{53}\text{Fe}$ and $^{140}\text{Ce}(p, d)^{140}\text{Ce}$ reactions at 122 MeV. *Nucl. Phys. A* **441**, 189–208 (1985). [https://doi.org/10.1016/0375-9474\(85\)90029-6](https://doi.org/10.1016/0375-9474(85)90029-6)

56. J.H. Polane, W.F. Feix, P.J. van Hall et al., The (p, d) reaction on ^{56}Fe at 24.6 MeV. *J. Phys. G: Nucl. Part. Phys.* **15**, 1735 (1989). <https://doi.org/10.1088/0954-3899/15/11/017>
57. H. Ohnuma, T. Suehiro, M. Sekiguchi et al., (p, d) Reactions at 52 MeV. I. $^{58}\text{Ni}(p, d)^{57}\text{Ni}$ (experimental). *J. Phys. Soc. Jpn.* **36**, 1236–1244 (1974). <https://doi.org/10.1143/JPSJ.36.1236>
58. K. Hosono, M. Kondo, T. Saito et al., A study of the (p, d) reactions on $A = 12$ –94 nuclei by 65 MeV polarized protons. *Nucl. Phys. A* **343**, 234–248 (1980). [https://doi.org/10.1016/0375-9474\(80\)90652-1](https://doi.org/10.1016/0375-9474(80)90652-1)
59. H. Nann, D.W. Miller, W.W. Jacobs et al., Systematics of (\vec{p}, d) analyzing powers at 94 MeV. *Phys. Rev. C* **27**, 1073–1077 (1983). <https://doi.org/10.1103/PhysRevC.27.1073>
60. G. Duhamel-Chrétien, G. Perrin, C. Perrin et al., Neutron hole states in ^{89}Zr via the $(p \rightarrow, d)$ reaction at 58 MeV. *Phys. Rev. C* **43**, 1116–1126 (1991). <https://doi.org/10.1103/PhysRevC.43.1116>
61. G.M. Crawley, J. Kasagi, S. Gales et al., Spin of deep hole states from (p, d) reactions. *Phys. Rev. C* **23**, 1818–1821 (1981). <https://doi.org/10.1103/PhysRevC.23.1818>
62. R.E. Anderson, J.J. Kraushaar, J.R. Shepard et al., A study of the ^{58}Ni , ^{90}Zr and $^{208}\text{Pb}(p, d)$ reactions at 121 MeV. *Nucl. Phys. A* **311**, 93–117 (1978). [https://doi.org/10.1016/0375-9474\(78\)90504-3](https://doi.org/10.1016/0375-9474(78)90504-3)
63. S.A. Dickey, J.J. Kraushaar, M.A. Rumore, The $^{102}\text{Ru}(p, d)^{101}\text{Ru}$ reaction at 26.3 MeV. *J. Phys. G: Nucl. Phys.* **12**, 745 (1986). <https://doi.org/10.1088/0305-4616/12/8/011>
64. L. Gan, H.B. Sun, Z.H. Li et al., Experimental study of the spectroscopic factors of $^{116-125}\text{Sn}$. *Phys. Rev. C* **101**, 014612 (2020). <https://doi.org/10.1103/PhysRevC.101.014612>
65. S.A. Dickey, J.J. Kraushaar, M.A. Rumore, The energy dependence of the spectroscopic factors for the $^{208}\text{Pb}(p, d)^{207}\text{Pb}$ reaction. *Nucl. Phys. A* **391**, 413–431 (1982). <https://www.sciencedirect.com/science/article/pii/0375947482906170>. [https://doi.org/10.1016/0375-9474\(82\)90617-0](https://doi.org/10.1016/0375-9474(82)90617-0)
66. K. Yagi, T. Ishimatsu, Y. Ishizaki et al., The single-hole states in the $50 < N \leq 126$ shell with (p, d) reactions. *Nucl. Phys. A* **121**, 161–175 (1968). [https://doi.org/10.1016/0375-9474\(68\)90505-8](https://doi.org/10.1016/0375-9474(68)90505-8)
67. T. Ishimatsu, M. Niwano, N. Kawamura et al., A systematic study of the (p, d) strength for transitions to deeply bound hole states. *Nucl. Phys.* **336**, 205–218 (1980). [https://doi.org/10.1016/0375-9474\(80\)90620-X](https://doi.org/10.1016/0375-9474(80)90620-X)
68. Y. Toba, K. Nagano, Y. Aoki et al., Analyzing powers for (p, d) reactions on ^{208}Pb and $^{142,144}\text{Nd}$ exciting neutron-hole states at $E_p = 22.0$ MeV. *Nucl. Phys. A* **359**, 76–90 (1981). [https://doi.org/10.1016/0375-9474\(81\)90212-8](https://doi.org/10.1016/0375-9474(81)90212-8)
69. M. Matoba, K. Yamaguchi, K. Kurohmaru et al., Depletion of the $2f_{7/2}$ neutron hole state in ^{207}Pb . *Phys. Rev. C* **55**, 3152–3154 (1997). <https://doi.org/10.1103/PhysRevC.55.3152>
70. H.C. Lee, *Dissertation, Survey of Neutron Spectroscopic Factors and Asymmetry Dependence of Neutron Correlations in Transfer Reactions* (Department of Physics and Astronomy of Michigan State University, 2010)
71. A. Sanetullaev, M.B. Tsang, W.G. Lynch et al., Neutron spectroscopic factors of ^{55}Ni hole-states from (p, d) transfer reactions. *Phys. Lett. B* **736**, 137–141 (2014). <https://doi.org/10.1016/j.physletb.2014.07.003>
72. J. Lee, M.B. Tsang, D. Bazin et al., Neutron-proton asymmetry dependence of spectroscopic factors in Ar isotopes. *Phys. Rev. Lett.* **104**, 112701 (2010). <https://doi.org/10.1103/PhysRevLett.104.112701>
73. D.Y. Pang, A.M. Mukhamedzhanov, Asymptotic normalization coefficients and spectroscopic factors from deuteron stripping reactions. *Phys. Rev. C* **90**, 044611 (2014). <https://doi.org/10.1103/PhysRevC.90.044611>
74. M. Kawai, M. Kamimura, K. Takesako, Chapter V. Coupled-channels variational method for nuclear breakup and rearrangement processes. *Prog. Theor. Phys. Suppl.* **89**, 118–135 (1986). <https://doi.org/10.1143/PTPS.89.118>
75. J.A. Tostevin, A. Gade, Systematics of intermediate-energy single-nucleon removal cross sections. *Phys. Rev. C* **90**, 057602 (2014). <https://doi.org/10.1103/PhysRevC.90.057602>
76. J.A. Tostevin, A. Gade, Updated systematics of intermediate-energy single-nucleon removal cross sections. *Phys. Rev. C* **103**, 054610 (2021). <https://doi.org/10.1103/PhysRevC.103.054610>
77. S.T. Wang, Y.P. Xu, D.Y. Pang, Energy dependence of the reduced single-particle strength for strongly-bound proton removal on ^{16}C . *Phys. Scr.* **94**, 015302 (2019). <https://doi.org/10.1088/1402-4896/aaed64>
78. Y.Z. Sun, S.T. Wang, Z.Y. Sun et al., Single-neutron removal from $^{14,15,16}\text{C}$ near 240 MeV/nucleon. *Phys. Rev. C* **104**, 014310 (2021). <https://doi.org/10.1103/PhysRevC.104.014310>
79. Y.Z. Sun, S.T. Wang, Y.P. Xu et al., Spectroscopic strength reduction of intermediate-energy single-proton removal from oxygen isotopes. *Phys. Rev. C* **106**, 034614 (2022). <https://doi.org/10.1103/PhysRevC.106.034614>
80. C. Wen, Y.P. Xu, D.Y. Pang et al., Quenching of neutron spectroscopic factors of radioactive carbon isotopes with knockout reactions within a wide energy range. *Chin. Phys. C* **41**, 054104 (2017). <https://doi.org/10.1088/1674-1137/41/5/054104>
81. Y.P. Xu, D.Y. Pang, X.Y. Yun et al., Proton-neutron asymmetry independence of reduced single-particle strengths derived from (p, d) reactions. *Phys. Lett. B* **790**, 308–313 (2019). <https://doi.org/10.1016/j.physletb.2019.01.034>
82. J. Manfredi, J. Lee, A.M. Rogers et al., Quenching of single-particle strengths in direct reactions. *Phys. Rev. C* **104**, 024608 (2021). <https://doi.org/10.1103/PhysRevC.104.024608>
83. Y.P. Xu, D.Y. Pang, C.X. Yuan et al., Quenching of single-particle strengths of carbon isotopes $^{9-12,14-20}\text{C}$ with knockout reactions for incident energies 43–2100 MeV/nucleon. *Chin. Phys. C* **46**, 064102 (2022). <https://doi.org/10.1088/1674-1137/ac5236>
84. B.A. Brown, New Skyrme interaction for normal and exotic nuclei. *Phys. Rev. C* **58**, 220–231 (1998). <https://doi.org/10.1103/PhysRevC.58.220>
85. J.A. Tostevin, University of Surrey version of the code TWOFNR (of M. Toyama, M. Igarashi and N. Kishida) and code FRONT(private communication)
86. C. Hebborn, F.M. Nunes, G. Potel et al., Optical potentials for the rare-isotope beam era. *J. Phys. G: Nucl. Part. Phys.* **50**, 060501 (2023). <https://doi.org/10.1088/1361-6471/acc348>
87. L. Yang, C.J. Lin, H.M. Jia et al., Progress on nuclear reactions and related nuclear structure at low energies. *Nucl. Tech.* **46**, 080006 (2023). <http://www.hjs.sinap.ac.cn/thesisDetails#10.11889/j.0253-3219.2023.hjs.46.080020> &lang=zh. <https://doi.org/10.11889/j.0253-3219.2023.hjs.46.080006>(Chinese)
88. Y. Chen, Y.L. Ye, K. Wei, Progress and perspective of the research on exotic structures of unstable nuclei. *Nucl. Tech.* **46**, 080020 (2023). <https://doi.org/10.11889/j.0253-3219.2023.hjs.46.080020>(Chinese)
89. R.H. McCamis, T.N. Nasr, J. Birchall et al., Elastic scattering of protons from $^{40,42,44,48}\text{Ca}$ from 20 to 50 MeV and nuclear matter radii. *Phys. Rev. C* **33**, 1624–1633 (1986). <https://doi.org/10.1103/PhysRevC.33.1624>
90. E.E. Gross, R.H. Bassel, L.N. Blumberg et al., Energy dependence of the elastic scattering and polarization of protons on ^{40}Ca . *Nucl. Phys. A* **102**, 673–680 (1967). <https://www.sciencedirect.com/science/article/pii/0375947467904022>. [https://doi.org/10.1016/0375-9474\(67\)90402-2](https://doi.org/10.1016/0375-9474(67)90402-2)
91. A. Nadasen, P. Schwandt, P.P. Singh et al., Elastic scattering of 80–180 MeV protons and the proton-nucleus optical potential. *Phys. Rev. C* **23**, 1023–1043 (1981). <https://doi.org/10.1103/PhysRevC.23.1023>

92. V. Comparat, R. Frascaria, N. Marty et al., Proton-nucleus elastic scattering at 156 MeV. Nucl. Phys. A **221**, 403–413 (1974). [https://doi.org/10.1016/0375-9474\(74\)90327-3](https://doi.org/10.1016/0375-9474(74)90327-3)
93. P. Schwandt, H.O. Meyer, W.W. Jacobs et al., Analyzing power of proton-nucleus elastic scattering between 80 and 180 MeV. Phys. Rev. C **26**, 55–64 (1982). <https://doi.org/10.1103/PhysRevC.26.55>
94. J.Z. Han, S. Xu, A. Jalili et al., Investigation of the level spectra of nuclei in the northeast region of doubly magic ^{40}Ca with intruder orbit $g_{9/2}$. Nucl. Sci. Tech. **34**, 85 (2023). <https://doi.org/10.1007/s41365-023-01243-x>

Springer Nature or its licensor (e.g. a society or other partner) holds exclusive rights to this article under a publishing agreement with the author(s) or other rightsholder(s); author self-archiving of the accepted manuscript version of this article is solely governed by the terms of such publishing agreement and applicable law.